A Multi-Receiver MHz WPT System with Hybrid Coupler

Yaoxia Shao[1], Ming Liu*[2], Chengbin Ma[1]
[1]University of Michigan-Shanghai Jiao Tong University Joint Institute, Shanghai, China
[2]School of Electronic Information and Electrical Engineering, Shanghai Jiao Tong University, Shanghai, China
yaoxiashao@sjtu.edu.cn, mingliu@sjtu.edu.cn, chbma@sjtu.edu.cn

***Abstract*—The megahertz (MHz) operating frequency increases the spatial freedom, making it more suitable for multi-receiver wireless power transfer (WPT) scenarios. Generally, in a single-receiver WPT system, similar shapes (e.g. spiral) of the transmitting coil and the receiving coil help to improve the cross coupling. However, in multi-receiver cases, traditional spiral receiving coils limit the maximum number of receivers, and the coil coupling varies obviously as position changes. This paper proposes a hybrid coupler of a spiral transmitting (Tx) coil and solenoid receiving (Rx) coils, which can effectively increase the upper limit of the number of receivers, and is also suitable for some receivers with special shapes (e.g. tubular). In addition, a new design method for the impedance matching network (IMN) of MHz WPT systems, which improves the robustness of the systems when the number of receivers varies, is also proposed.**

***Index Terms*—Solenoid, multi-receiver, MHz, wireless power transfer (WPT), impedance matching.**

I. Introduction

Wireless power transfer (WPT) through magnetic coupling has a profound impact on both consumer electronics and industrial applications [1]. Compared with traditional plug-in systems, WPT systems are free of cables, providing users with a more convenient, safe and efficient experience [2]. Currently, most of commercialized WPT systems operate in kHz band, such as at several hundreds kHz [3]. It is mainly because this frequency band provides a richer selection of power electronics components. However, the kHz operation requires large-size coupling coils and ferrite to achieve enough mutual inductance.

WPT systems with higher operation frequency, such as several MHz, own the potential to be lighter and more compact [4]. Meanwhile, increasing the frequency brings a higher level of spacial freedom [5], which is beneficial to realize multi-receiver WPT systems. There are few researches on the design and optimization for multi-receiver MHz WPT systems [6]–[8]. The existing multi-receiving system is faced with defects such as poor robustness and low capacity of receiving coils. This paper proposes a new hybrid coupler with a spiral transmitting (Tx) coil and solenoid receiving (Rx) coils, increasing the arrangement density of the receivers. Meanwhile, this design reduces the restrictions on the shape of the receivers, such as tubular and spherical appliances can also be charged. Furthermore, the concept of wireless outlets can be extended from the hybrid coupler. Fig. 1 illustrates the conventional outlet with the wired plug and the wireless outlet realized by the hybrid coupler. This concept offers an alternative to more convenient, safe and reliable power supply method, which also has application prospect in smart home, consumer electronic products and other fields.

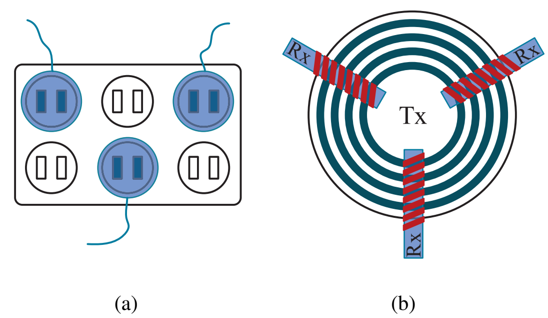

Fig. 1. Two types of outlets. (a) Conventional outlet. (b) Proposed wireless outlet.

Multi-receiver MHz WPT systems are also faced with unique technical challenges, one of them is potentially higher switching loss due to high-frequency operation [9]. Class E PAs and rectifiers are promising candidate to solve this issue, thanks to their soft-switching property [10]. As such, this paper use single-end Class E PA and full-wave current-driven Class E rectifier as power conversion stages for the transmitter and receivers.

Another challenge for such a system is the dynamic reflected impedance seen by the PA, caused by changes in the number of receivers. And the Class E PA is naturally not robust against pure-resistive load change. To solve this, a novel method to explicitly design impedance matching networks (IMN) for MHZ WPT systems is proposed, based on mathematical modeling and simplification.

Section II gives the derivation of the method to design the IMNs. System configuration and parameter design process is introduced in Section III. The hybrid coupler is proposed in Section IV. In Section V, an experimental system is built for verification. Finally, Section VI concludes the paper.

II. A Novel Method to Design Impedance Matching Networks for MHz WPT Systems

Well-designed IMNs predispose MHz WPT systems to more useful characteristics, such as LIO, high tolerance to coil misalignment, and high robustness in multi-receiver scenarios.

We start the derivation by supposing the IMN to be the T-network in Fig. 2. Thus the transformed impedance, i.e., the input impedance of the IMN, can be calculated as:

$$\begin{aligned} Z_{net} &= R_{net} + jX_{net} = Z_{T1} + (Z_{load} + Z_{T2})//Z_{T3} \\ &= jX_{T1} + \frac{jX_{T3}(R_{load} + jX_{load} + jX_{T2})}{R_{load} + jX_{load} + jX_{T2} + jX_{T3}} \end{aligned} \quad (1)$$

where Z_{load} represents the impedance seen by the IMN, and $X_{T1}{\sim}X_{T3}$ represent the reactance of $Z_{T1}{\sim}Z_{T3}$.

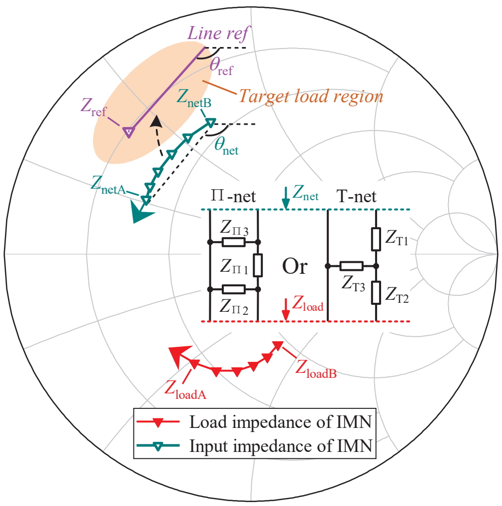

Fig. 2. Schematic diagram of IMN design for MHz WPT applications.

As shown in Fig. 2, the arrows at the head of impedance curves imply the direction of impedance variation, and a reference line (line ref) is set in the target load region to help locate the Z_{net} curve. In the case of single frequency, a lossless 2-port network has only 3 independent design variables, which indicates the cascade of T-networks and Π-networks will not increase the design freedom of IMN, in terms of impedance transformation. Apparently, these 3 design variables of IMNs are insufficient to totally manipulate the position of Z_{net} curve.

Therefore, the Z_{net} curve, which represent a varying impedance, must be quantified within 3 dimensions to make it possible to design the IMN explicitly, i.e., by solving a system of equations. This can be achieved by determining the coordinates of the head of Z_{net} curve and the angle of the line connecting the head and the tail of Z_{net} curve:

$$\begin{aligned} Z_{netA} = Z_{ref} \ &\Rightarrow \begin{cases} R_{netA} = R_{ref}, \\ X_{netA} = X_{ref}, \end{cases} \\ \theta_{net} = \theta_{ref} \ &\Rightarrow \angle(Z_{netA} - Z_{netB}) = \theta_{ref}, \end{aligned} \quad (2)$$

where Z_{netA}, Z_{netB} and Z_{ref} represent the head, the tail of Z_{net} curve and the head of the reference line, respectively. The equation above implies that the head and the tail of Z_{load} curve have different "matching priority". Literally, the head Z_{loadA} is more important since the position of its corresponding head Z_{netA} can be matched to the point Z_{ref}, while the tail Z_{netB} is only guaranteed to lie on the reference line. For example, it is reasonable to set the impedance correlated to the maximum output power as the head of the curve.

With the substitution of (1) into (2), one may solve for the parameters of the IMN that can transform Z_{load} onto the reference line:

$$\begin{cases} X_{T1} = -\frac{(a \pm c)R_{ref}}{2eR_{loadA}} + \sqrt{\frac{(\pm ac + bf)R_{ref}}{2e^2 R_{loadA}}} + X_{ref} \\ X_{T2} = \frac{1}{2}\left(\frac{\pm a + d}{e} + \sqrt{\frac{2(\pm ac + bf)R_{ref}}{e^2 R_{loadA}}}\right) - X_{loadB} \\ X_{T3} = -\sqrt{\frac{(\pm ac + bf)R_{ref}}{2c^2 R_{loadA}}} \end{cases}$$
$$\pm : \begin{cases} + & \theta_{ref} \in \left(-\frac{\pi}{2}, \frac{\pi}{2}\right), \\ - & \theta_{ref} \in \left(-\pi, -\frac{\pi}{2}\right) \cup \left(\frac{\pi}{2}, \pi\right], \end{cases} \quad (3)$$

where $a{\sim}f$ are intermediate variables defined in (4). For simplicity, the solutions when $\theta_{ref} = \pm\frac{\pi}{2}$ are not listed, which can be obtained by taking the limit. Furthermore, the calculated T-network can be easily transformed to a Π-network shown in Fig. 2:

$$\begin{cases} X_{\Pi 1} = X_{T1} + X_{T2} + \frac{X_{T1}X_{T2}}{X_{T3}}, \\ X_{\Pi 2} = X_{T2} + X_{T3} + \frac{X_{T2}X_{T3}}{X_{T1}}, \\ X_{\Pi 3} = X_{T3} + X_{T1} + \frac{X_{T3}X_{T1}}{X_{T2}}. \end{cases} \quad (5)$$

From (3)∼(5), an explicit method to design IMNs for MHZ WPT systems is obtained. It should be pointed out that the method proposed in this paper exhausts the potential of the

$$\begin{aligned} a =& \sqrt{(R_{loadA} + R_{loadB})^2 + (X_{loadA} - X_{loadB})^2 + 4R_{loadA}R_{loadB}\tan^2\theta_{ref}}\sqrt{(R_{loadA} - R_{loadB})^2 + (X_{loadA} - X_{loadB})^2} \\ b =& R_{loadB}^2 + R_{loadA}^2\left(1 + 2\tan^2\theta_{ref}\right) + (X_{loadA} - X_{loadB})^2 + \\ & 2R_{loadA}\left[R_{loadB}\left(1 + \tan^2\theta_{ref}\right) + \tan\theta_{ref}\left(X_{loadB} - X_{loadA}\right)\right] \\ c =& R_{loadA}^2 - R_{loadB}^2 - (X_{loadA} - X_{loadB})^2 + 2R_{loadA}\left(X_{loadA} - X_{loadB}\right)\tan\theta_{ref} \\ d =& R_{loadA}^2 - R_{loadB}^2 + (X_{loadA} - X_{loadB})^2 + 2R_{loadA}\left(X_{loadA} - X_{loadB}\right)\tan\theta_{ref} \\ e =& R_{loadA}\tan\theta_{ref} - R_{loadB}\tan\theta_{ref} - X_{loadA} + X_{loadB} \\ f =& (R_{loadA} - R_{loadB})^2 + (X_{loadA} - X_{loadB})^2 \end{aligned} \quad (4)$$

2-port IMN, but there are still other strategy to establish equations.

III. Parameter Design

A. System Configuration

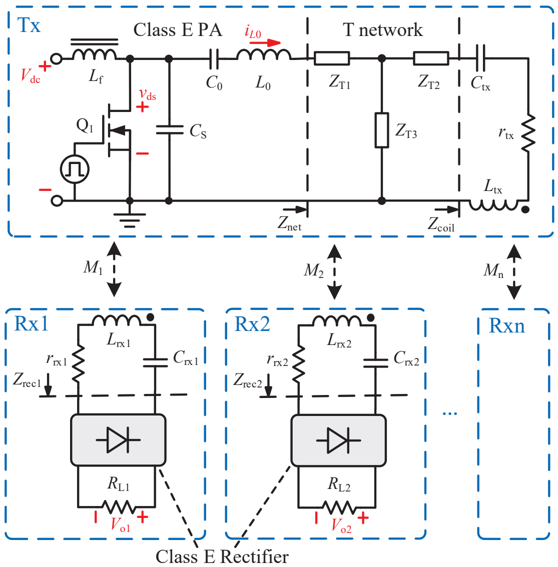

Fig. 3. System configuration of proposed multi-receiver MHz WPT system.

Fig. 3 illustrates configuration of the proposed multi-receiver MHz WPT system, which is composed of a PA, an IMN of T-network, a transmitting (Tx) coil and several receiving (Rx) coils connected with corresponding rectifiers. In this system, Class E typology is applied in both the PA and the rectifier, due to its zero voltage switching (ZVS) and zero voltage derivative switching (ZVDS) characteristics. In the figure, $M_1 \sim M_n$ are the mutual inductance between the Tx coil and different Rx coils, with the cross coupling between the Rx coils ignored. L_{tx} is inductance of the Tx coil and $L_{rx1} \sim L_{rxn}$ are the inductances of Rx coils. Their parasitic resistors and compensation capacitors are also shown in the figure.

B. Rectifier and Compensation of Coils

The configuration of full-wave current-driven Class E rectifier is shown in Fig. 4. The rectifier of i-th receiver consists of 2 diodes D_r, 2 parallel capacitors C_{ri}, 2 filter inductors L_r, a filter capacitor C_L, and a dc load R_{Li}. The input resistance and reactance of the Class E full-wave reactance can be calculated as:

$$R_{reci} = \frac{1}{2\pi\omega C_{ri}} \left[4 - 4\cos\left(2\pi D_i\right) - \cos\left(2\phi_i + 4\pi D_i\right) + \cos 2\phi_i + 8\pi\left(1 - D_i\right)\sin\left(\phi_i + 2\pi D_i\right)\cos\phi_i\right], \tag{6}$$

$$X_{reci} = \frac{1}{2\pi\omega C_{ri}} \left[\sin\left(2\phi_i + 4\pi D_i\right) - 4\sin\left(2\pi D_i\right) - \sin\phi_i + 4\pi\left(D_i - 1\right)\left(1 + 2\sin\left(\phi_i + 2\pi D_i\right)\right)\sin\phi_i\right], \tag{7}$$

where ω is the operating frequency, D_i is the duty cycle of the diodes, and ϕ_i is the initial phase angle of the rectifier current. The compensation capacitor of the Rx coil, C_{rxi}, is designed to eliminate the reactance of the receiver, which caused by the inductance of Rx coil and the input reactance the rectifier:

$$X_{reci} + \omega L_{rxi} - \frac{1}{\omega C_{rxi}} = 0. \tag{8}$$

Therefore, the input impedance of the Tx coil, Z_{coil}, can be calculated as the sum of r_{tx} and the reflect impedance:

$$Z_{coil} = r_{tx} + Z_{rft} = r_{tx} + \sum_{i=1}^{n} \frac{\omega^2 M_i^2}{R_{reci} + r_{rxi}}. \tag{9}$$

Note that C_{tx} is designed to be resonant with L_{tx} at ω, thus Z_{coil} is pure resistive.

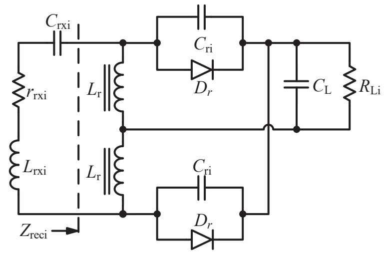

Fig. 4. Full-wave current-driven Class E rectifier.

C. Power Amplifier and Impedance Matching Network

Load-pull is an effective technique to portray the overall characteristics of a PA as the load changes. Fig. 5 shows the load-pull simulation results of the single-end Class E PA when L_0 is resonant with C_0, and $C_s = 287$ pF. A well-known RF simulation software, advanced design system (ADS) from Agilent is used. In the Smith Chart, the contours represent the normalized output power and efficiency of PAs under different load impedances. The normalized output power of the PA is defined as:

$$P_{net,norm} = \frac{P_{net}}{V_{dc}^2}, \tag{10}$$

where P_{net}, V_{dc} are the input power of the T-network and the dc supply voltage of the PA, respectively.

Suppose there are 1$\sim$3 same receivers put on the Tx coil, each of them brings 9 Ω pure resistive reflect impedance (same with the experimental setting in section V), which is calculated by (9). Then, if the parasitic resistance of the coil, r_{tx} is ignored, the input impedance of the coil Z_{coil} varies between 9$\sim$27 Ω, as shown by the red line in Fig. 5. It is reasonable to equate the high-efficiency region in the Smith Chart with "soft-switching region". Therefore, the primary function of the IMN is to transform the Z_{coil} curve into the high efficiency region, bounded by 95 % PA efficiency contour. Moreover, the PA output power is supposed to be proportional to the number of receivers, to ensure constant voltage outputs. To meet the above 2 conditions, the reference line is set as shown by the purple line in the figure. The

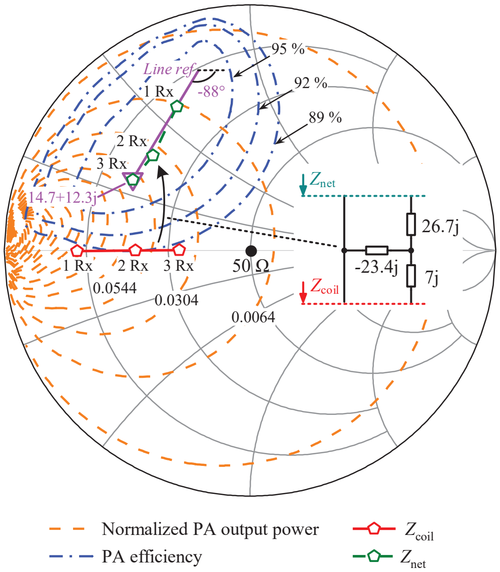

Fig. 5. Load-pull results of single-end Class E PA and impedance matching of multi-receiver WPT system (L_0 is resonant with C_0 at ω, $C_s = 287$ pF).

TABLE I
TARGET SETTING AND CALCULATED PARAMETERS OF THE IMN

Original Impedances	
Z_{loadA} (Z_{coilA})	27+0j Ω
Z_{loadB} (Z_{coilB})	9+0j Ω
Target Setting	
Z_{ref}	14.7+12.3j Ω
θ_{ref}	-88°
Calculated T-net	
Z_{T1}	26.7j Ω
Z_{T1}	7j Ω
Z_{T1}	-23.4j Ω

variables to quantify the original loads, the reference line and the IMN calculated by (3)∼(4) are listed in Table I. The settings in the Table ensure that the Z_{coil} corresponding to more receivers is transformed to Z_{net} corresponding to higher PA output power.

IV. Hybrid Coupling Coils

For multi-receiver WPT systems, a new hybrid coupler is proposed, with a spiral Tx coil and a solenoid Rx coil. Fig. 6 compares the proposed hybrid coupler and the conventional ones. The essential difference between the 2 couplers is that the former uses the radial component of the magnetic field generated by the Tx coil while the latter uses the axial one. As shown in Fig. 7, the radial magnetic flux density performs better homogeneity than the axial one. In another word, the change of cross coupling caused by the movement of the Rx coil is reduced with the new coupler. Moreover, when the trace spacing of the Tx coil is high enough, the high magnetic flux density area of the radial magnetic field is larger than that of the axial one.

Based on the above factors and the preliminary simulations, the hybrid coupler has the following 4 advantages:

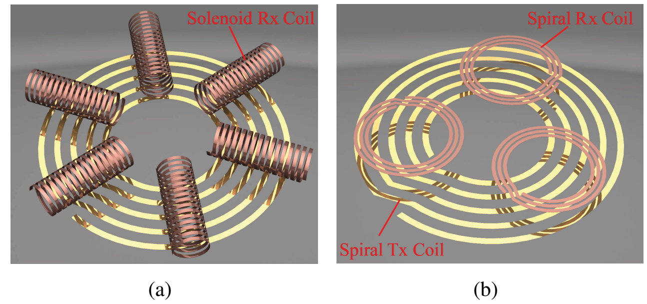

Fig. 6. Coupler with 2 types of Rx coils. (a) Proposed solenoid Rx coil. (b) Conventional spiral Rx coil.

- Higher receiver capacity: Due to the larger area of high magnetic flux density and tubular shape of Rx coils, the same charging area can accommodate more receivers;
- Suitable for those receivers with special shapes: The Rx coil can be attached to the surface of the appliances;
- High tolerance to the change of relative position of the coils: The radial magnetic field has better homogeneity;
- Higher mutual inductance increment brought by ferrite sheet: The ferrite has greater gain on the magnetic field parallel to it, i.e., the radial component of magnetic field.

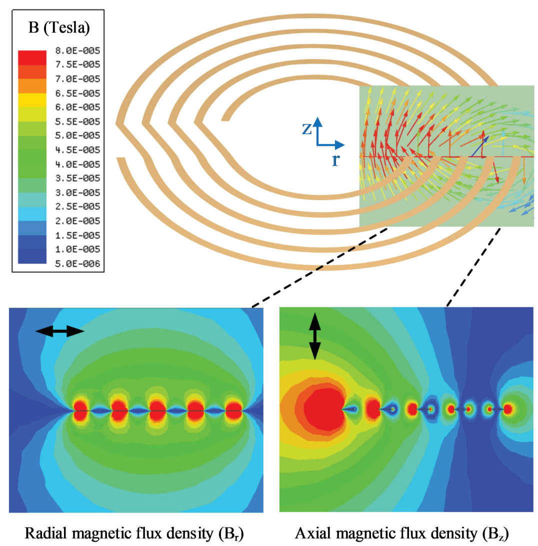

Fig. 7. Radial and axial components of magnetic flux density of a spiral coil.

V. Experimental Verification

A demo multi-receiver MHz WPT system with the proposed hybrid coupler is shown in Fig. 8. 12V, 5W LED strips are used as the loads of the receivers. Each receiver is compensated to be pure resistive by (8), bringing 9 Ω reflect impedance. Therefore, the optimal parameters of the IMN is already given in Table I. In order not to hide the light of the LED strips, ferrite sheets only cover the the lower surface of the LED tubes. Moreover, an acrylic plate with grooves is attached to the Tx coil, which steers the receivers in the radial direction.

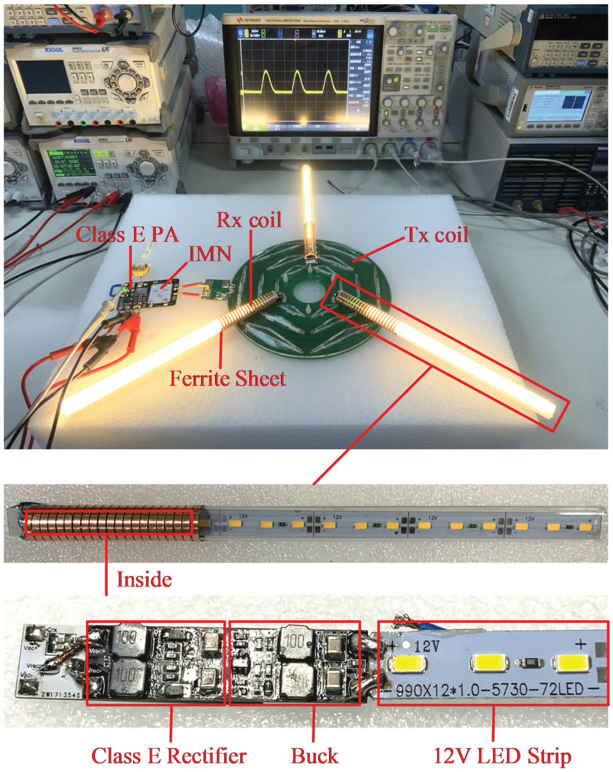

Fig. 8. Experimental setup of the multi-receiver MHz WPT system.

It is worthy noting that Z_{T1} and Z_{T2} of the IMN can be combined to the PA and the Tx coil, respectively, as shown in Fig. 9. "*" indicates the the value of corresponding component changes after combination. Therefore, the T-network only requires one additional component (C_{T3}), which benefits the compactness of the transmitter. Parameters of the experimental system are listed in Table II.

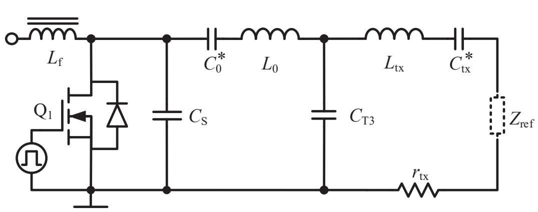

Fig. 9. Circuit of the transmitter after component combination.

To validate the robustness of the systems when the number of receivers varies, V_{ds} waveforms with different number of receivers are tested (Fig. 10), where the blue curves are original and the red curves are after de-noising. It can be clearly seen that the soft switching property is maintained well, thanks to the proposed IMN design method. The system efficiency is maintained between 79 %∼84 % as number of the receivers varies between 1∼3.

TABLE II
PARAMETERS OF THE EXPERIMENTAL SYSTEM

Parameters	Value	
f	6.78 MHz	
L_f	10 uH	
L_0	2.17 uH	
C_0^*	357 pF	$\Longrightarrow$ Z_{T1} = 26.7j Ω
C_s	287 pF	
L_{tx}	6.65 uH	
C_{tx}^*	85 pF	$\Longrightarrow$ Z_{T2} = 7j Ω
r_{tx}	1.1 Ω	
C_{T3}	1005 pF	$\Longrightarrow$ Z_{T3} = -23.4j Ω
Z_{ref}	9∼27 Ω	
$M_1 \sim M_3$	0.45 uH	
L_r	4.7 uH	
$C_{r1} \sim C_{r3}$	540 pF	
C_L	10 uF	
$R_{L1} \sim R_{L3}$	40 Ω	

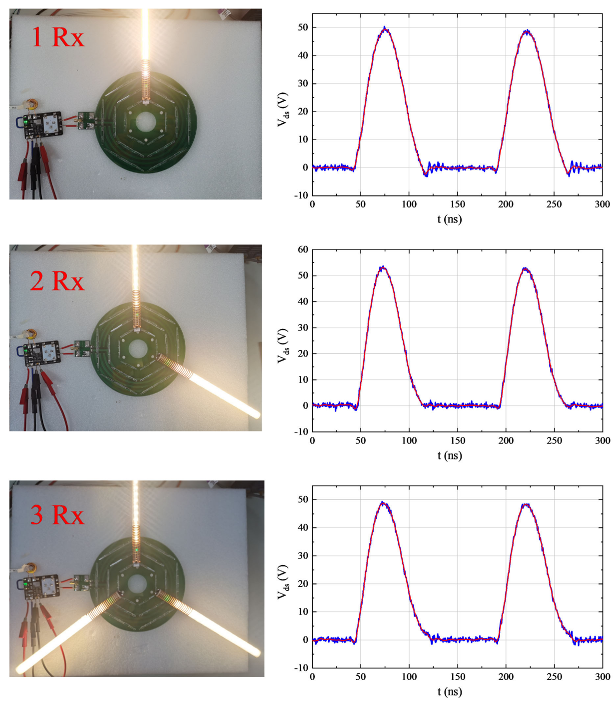

Fig. 10. Drain-source voltage V_{ds} of the Class E PA under different number of receivers.

VI. CONCLUSIONS

A multi-receiver MHz WPT system with hybrid coupler is proposed. This system has the potential to broaden the application scenarios of multi-receiver WPT technology. Issues such as IMN design are solved and detailed parameter design method is given. Subsequent research will focus on more complicated conditions such as variations of dc load and mutual-inductance.

REFERENCES

[1] Y. Jang and M. M. Jovanovic, "A contactless electrical energy transmission system for portable-telephone battery chargers," *IEEE Transactions on Industrial Electronics*, vol. 50, no. 3, pp. 520–527, 2003.

[2] M. Liu, H. Zhang, Y. Shao, J. Song, and C. Ma, "High-performance megahertz wireless power transfer: Topologies, modeling, and design," *IEEE Industrial Electronics Magazine*, 2020.

[3] Z. Li, C. Zhu, J. Jiang, K. Song, and G. Wei, "A 3-kw wireless power transfer system for sightseeing car supercapacitor charge," *IEEE Transactions on Power Electronics*, vol. 32, no. 5, pp. 3301–3316, 2016.

[4] S. Y. R. Hui, W. Zhong, and C. K. Lee, "A critical review of recent progress in mid-range wireless power transfer," *IEEE Transactions on Power Electronics*, vol. 29, no. 9, pp. 4500–4511, 2013.

[5] A. Kurs, A. Karalis, R. Moffatt, J. D. Joannopoulos, P. Fisher, and M. Soljačić, "Wireless power transfer via strongly coupled magnetic resonances," *science*, vol. 317, no. 5834, pp. 83–86, 2007.

[6] M. Liu and M. Chen, "Dual-band multi-receiver wireless power transfer with reactance steering network," in *2018 IEEE PELS Workshop on Emerging Technologies: Wireless Power Transfer (Wow)*. IEEE, 2018, pp. 1–6.

[7] C. Peng, Z. Chen, Z. Liu, J.-F. Wang, J. Liang, C. Li, S. Tao, and J. Li, "On the load-independence of a multi-receiver wireless power transfer system," *IEEE Microwave and Wireless Components Letters*, vol. 29, no. 8, pp. 563–565, 2019.

[8] A. Uchida, S. Shimokawa, and H. Oshima, "Effect of load dependence of efficiency in a multi-receiver wpt system," in *2017 IEEE Wireless Power Transfer Conference (WPTC)*. IEEE, 2017, pp. 1–4.

[9] Y. Shao, M. Liu, H. Zhang, and C. Ma, "Dual-band wireless power transmitter with reconfigurable power amplifier and" decoupling ring"," in *IECON 2020 The 46th Annual Conference of the IEEE Industrial Electronics Society*. IEEE, 2020, pp. 3889–3894.

[10] F. Raab, "Idealized operation of the class e tuned power amplifier," *IEEE transactions on Circuits and Systems*, vol. 24, no. 12, pp. 725–735, 1977.

[11] X. Dai, X. Li, Y. Li, and A. P. Hu, "Maximum efficiency tracking for wireless power transfer systems with dynamic coupling coefficient estimation," *IEEE Transactions on Power Electronics*, vol. 33, no. 6, pp. 5005–5015, 2017.

[12] X. Qu, H. Han, S.-C. Wong, K. T. Chi, and W. Chen, "Hybrid ipt topologies with constant current or constant voltage output for battery charging applications," *IEEE Transactions on Power Electronics*, vol. 30, no. 11, pp. 6329–6337, 2015.